NANO LETTERS

2006
Vol. 6, No. 4
605−610

Surface Chemistry Controls Crystallinity of ZnS Nanoparticles

Benjamin Gilbert,*,† Feng Huang,‡ Zhang Lin,‡ Carmen Goodell,† Hengzhong Zhang,† and Jillian F. Banfield†

Department of Earth and Planetary Sciences, University of California, Berkeley, California 94720, and Fujian Institute of Research on the Structure of Matter, Chinese Academy of Sciences, Fuzhou, Fujian, 350002, People's Republic of China

Received November 8, 2005; Revised Manuscript Received February 6, 2006

ABSTRACT

Combined small-angle and high energy wide-angle X-ray scattering measurements of nanoparticle size and structure permit interior strain and disorder to be observed directly in the real-space pair distribution function (PDF). PDF analysis showed that samples of ZnS nanoparticles with similar mean diameters (3.2–3.6 nm) but synthesized and treated with different low-temperature procedures possess a dramatic range of interior disorder. We used Fourier transform infrared spectroscopy to detect the surface species and the nature of surface chemical interactions. Our results suggest that there is a direct correlation between the strength of surface-ligand interactions and interior crystallinity.

Introduction. Inorganic nanoparticles are a distinct class of matter because their properties can be substantially modified relative to the bulk material. In some systems, typified by the cadmium chalcogenides, quantum confinement (a pure size effect) leads to size-tunable electronic behavior.[1,2] For other substances, including many metal oxides, nanoparticles are found to adopt a structural phase that is metastable in the bulk.[3,4] Thus, the properties of nanoparticles are a function of both size and size-induced structural effects.

There are currently no experimental approaches that provide a complete description of nanoparticle structure. For example, although the crystal phase is obtained readily from diffraction methods, the presence of defects and disorder must generally be inferred from indirect measurements. Moreover, no method can currently reveal surface structure. Partly as a consequence of these practical challenges, it is frequently assumed that nanoparticles are defect-free and internally unstrained.

Theoretical descriptions of the electronic structure of nanoparticles that neglect the possible existence of structural disorder have proven to be highly successful.[5,6] Nevertheless, a number of theoretical[7,8] and experimental studies[9−11] have indicated that semiconductor nanoparticles may possess significant interior disorder. Disorder and defects can contribute significantly to the material and electronic properties of bulk crystals.[12,13] If present in nanoparticles, disorder and defects will significantly modify material properties, and hence there is a strong motivation for pursuing experimental approaches that are sensitive to the details of nanoparticle structure. EXAFS analyses of nanoparticles often showed the presence of excess static disorder in nanoparticles.[13,15,16] Debye Function Analysis has been applied to estimate stacking fault frequencies[17,18] and a pair distribution function (PDF) based analysis has been used to quantify internal strain in nanoparticles.[19] However, there is no general picture of the incidence and nature of crystalline imperfections in nanoparticles.

Although a great deal of attention has been given to controlling nanoparticle size and size distribution, it is less clear whether nanoparticle crystallinity is determined by temperature, the kinetics of the growth pathway, or by specific surface ligand interactions. There are strong experimental indications that nanoparticles are dynamic systems at room temperature. For example, complete cation exchange can occur extremely rapidly within CdSe nanoparticles in Ag solution;[20] solvent effects[9] or aggregation[21] can cause profound changes in nanoparticle structure; and oriented aggregation may lead to interface elimination and growth.[22−24] The implications of these findings are that surface interactions are the dominant factor in nanoparticle crystallinity and the thermodynamic stable structure of individual nanoparticles is kinetically accessible at room temperature.

Many experimental and theoretical studies have considered the interactions between nanoparticles and different types of surface ligands. Such work revealed that surface ligands

* Corresponding author. E-mail: bgilbert@lbl.gov. Present address: Earth Sciences Division, Lawrence Berkeley National Lab, Berkeley, CA 94720.
† University of California, Berkeley.
‡ Fujian Institute of Research on the Structure of Matter, Chinese Academy of Sciences.

10.1021/nl052201c CCC: $33.50
Published on Web 02/25/2006

can determine important properties, including optical absorption threshold position[16,25] and photoluminescence efficiency.[26] No correlation has been made, however, between the type of surface ligand and the detailed nanoparticle structure. Here we show that different types of interactions at the surface of ZnS nanoparticles can result in a very large range of internal crystallinity for nanoparticles of the same size.

Experimental Section. ZnS nanoparticles approximately 3 nm in diameter were synthesized by three methods, and with subsequent treatments we produced nanoparticles with four different surface environments. The syntheses and treatment are briefly described here. *Sample 1.* ZnS nanoparticles coated in mercaptoethanol ($SHCH_2CH_2OH$) were synthesized by combining aqueous solutions of Na_2S and $ZnCl_2$ at pH 10.2 in the presence of mercaptoethanol.[27] *Sample 2.* Na_2S in methanol was added dropwise to a solution of $ZnCl_2$ in anhydrous methanol with constant stirring. Washing with additional anhydrous methanol to remove NaCl results in a suspension of approximately 3 nm ZnS nanoparticles in pure methanol.[9] *Sample 3.* DI water was added to ZnS nanoparticles in methanol (i.e., sample 2) to give a final water concentration of 10% v/v. The interaction of water with the nanoparticle surface drives a structural transformation within the nanoparticles without change of particle size.[9] *Sample 4.* Uncoated ZnS nanoparticles in water were obtained by adding dropwise a solution of 4.8 g of Na_2S in 200 mL DI water to 2.7 g of $ZnCl_2$ in 300 mL DI water adjusted to pH 11 with NaOH. *Sample 5.* Pure synthetic bulk ZnS powder (greater than 100 nm grain size) was obtained by treating commercial sphalerite at 200 C in 1M NaOH in a hydrothermal bomb.

All nanoparticles from the above syntheses were determined by to be nanoscale from ultraviolet−visible (UV−vis) absorption spectroscopy. X-ray diffraction (XRD) measurements showed the nanoparticles to be in the zinc blende phase, with no detectable wurtzite component discernible in Rietveld refinement. A more precise determination of particle size was made with small-angle X-ray scattering (SAXS) measurements from diluted samples in the appropriate solvents.[29,30] The nanoparticle diameters obtained in this way were checked to be consistent with transmission electron microscopy (TEM), for example, Figure 1c and Figure S1.

SAXS measurements on the nanoparticle samples were performed at beamline 5-ID-D at the APS (samples 1−3) or beamline 1−4 at the SSRL (sample 4). Two-dimensional scattering patterns were corrected for detector background and the solvent contribution and integrated using standard methods.[28] ZnS nanoparticles synthesized without surface capping molecule (mercaptoethanol) were observed to aggregate. Thus, the SAXS curves were fitted by spherical particles with a Schultz distribution of diameters (see, e.g., ref 31) in an aggregate that is described by Teixeira's expression for fractal aggregates.[32] We checked that this expression gives accurate size determination in the presence of aggregation by comparing the results from sample 4 in both dispersed and aggregated states. The aggregated sample was prepared by slow evaporation of water from the sample until a gel was formed. Figure 1a and b shows the SAXS data and fits for all samples; the best-fit results are summarized in Table 1.

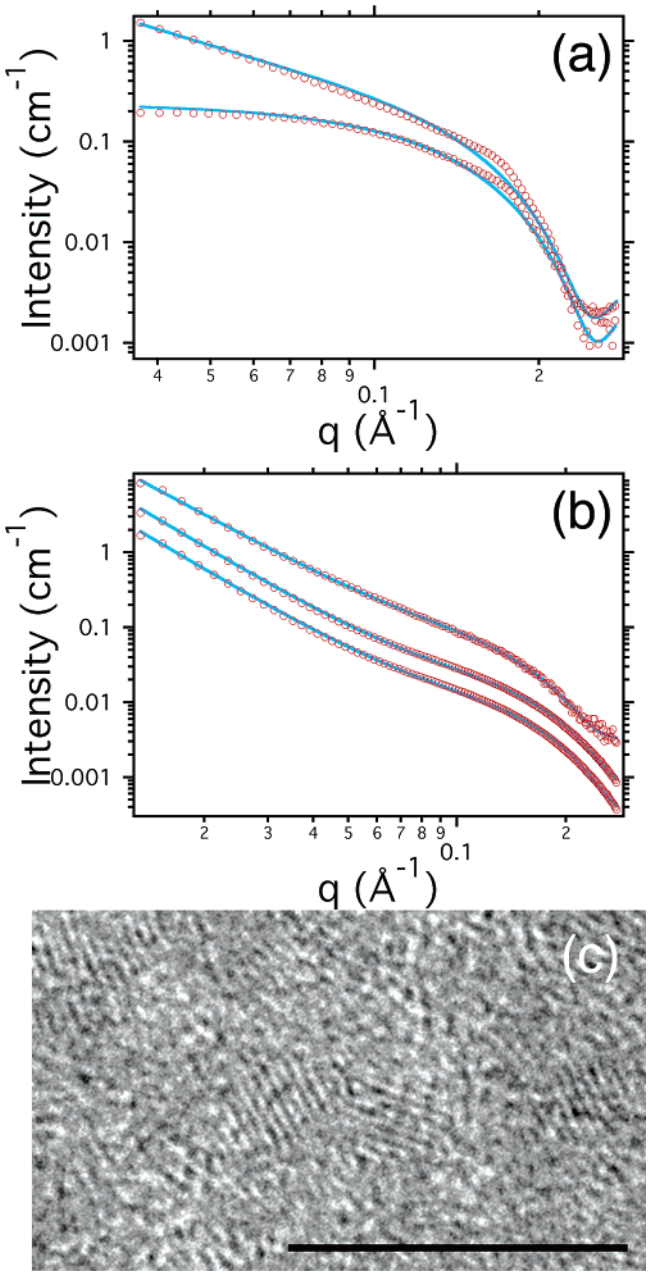

Figure 1. Small-angle X-ray scattering (SAXS) and transmission electron microscopy (TEM) determination of nanoparticle size. (a) SAXS patterns for mercaptoethanol-coated ZnS nanoparticles in a dilute dispersion (lower curve) or aggregated in a gel (sample 1). (b) SAXS patterns for ZnS nanoparticle aggregates in different solvents: in water at pH 10 (sample 4), in methanol (sample 2), and in 10% water in methanol (sample 3). Curves for samples 2 and 3 are offset for clarity. Circles = data; lines = fit. (c) TEM image of individual mercaptoethanol-coated ZnS nanoparticles (sample 4). At least three individual nanoparticles can be identified by lattice fringes. Scale bar = 10 nm.

Nanoparticle structure and disorder was determined using wide-angle X-ray scattering (WAXS) at beamline 11-ID-B at the APS with a photon energy of 93 keV and using a two-dimensional image plate detector.[33] WAXS patterns recording the scattering intensity vs diffraction vector

Table 1. Best-fit Parameters Following Fits to SAXS Data in Figure 1

sample number	1	1, agg	2	3	4
surface coating	SHEtOH	SHEtOH	methanol	water	oxidized
mean radius (Å)	17.4	17.6	14.3	14.5	16.1
radius spread (Å)	0.6	0.8	1.0	1.0	0.6
fractal dimension	n/a	2.2	2.6	2.6	2.1

magnitude, q, were acquired from ZnS nanoparticles as a suspension in the appropriate solvent (samples 1 and 2) or as a dried powder (samples 3−5). The magnitude of the diffraction vector $q = (4\pi/\lambda) \sin \theta$, where the X-ray wavelength $\lambda = 0.10775$ Å and 2θ is the scattering angle. The diffraction intensity was treated by subtracting the backgrounds from the sample cell and solvent (where applicable) and normalizing, using atomic form factors and Compton scattering factors obtained from the literature.[34,35] The smooth atomic scattering contribution to the intensity is removed to produce the structure factors for each sample, which possess all of the structural information. The structure factors were multiplied by the q scattering axis and Fourier transformed to give the real-space pair distribution functions (PDF).[36] Figure 2 shows the q-weighted structure factors and associated PDFs for each sample. Excess strain and disorder within spherical nanoparticles can be shown visually by comparing the PDF obtained for real nanoparticles with a PDF that is simulated for a powder of the bulk material but with the size of the real nanoparticles. This procedure is described below and in ref 19. For comparison, the experimental PDF for bulk ZnS is included in Figure 2.

The surface chemistry of the samples was analyzed with Fourier transform infrared spectroscopy (FTIR). The samples were dried in a vacuum oven at 50 °C, and then degassed at $\sim 1 \times 10^{-6}$ Torr overnight at 150 °C. Samples that were degassed at room temperature or at 150 °C gave identical XRD patterns, and no additional surface species were created by the high-temperature treatment. Furthermore, no loss of the mercaptoethanol species was seen from the FTIR signal, in agreement with high-temperature studies of Vogel et al.[27] The clean samples were placed in a dry N_2 atmosphere and portions were mixed with anhydrous KBr and pressed into a pellet for FTIR. FTIR was performed with a Nicolet 8700 spectrometer (32−1024 scans at a resolution of 4 cm^{-1}) with continuous flow of dry N_2. A blank KBr pellet was used as a reference for the handling procedure, and showed no detectable water contamination during sample handling and data acquisition.

Results and Discussion. Data from SAXS and TEM (Figure 1) and UV−vis absorption spectroscopy indicate that the ZnS nanoparticles in all four samples are of a similar size. As shown in Table 1, the mean nanoparticle radii vary between 14.3 and 17.6 Å.

All of the diffraction peaks from samples 1, 3, and 4 in Figure 2a can be attributed to the cubic sphalerite phase of ZnS, and Reitveld refinement did not detect a hexagonal (wurtzite) phase. However, the low stacking fault energy in ZnS leads to the facile formation of polytype structures that can be difficult to detect with X-ray diffraction alone. Stacking faults have been observed in TEM images of CdS

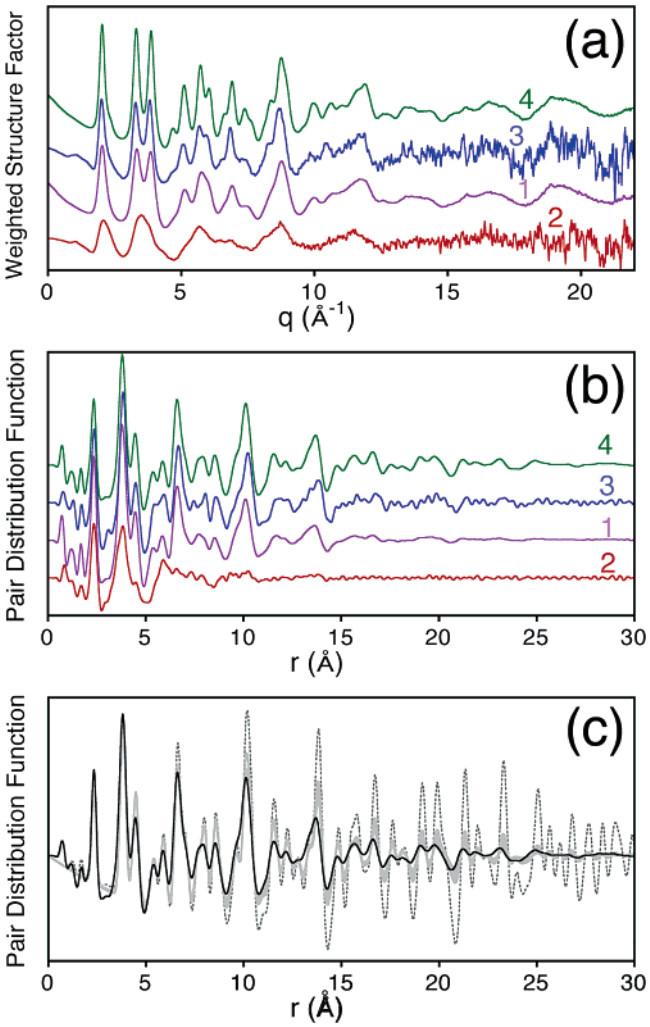

Figure 2. Wide-angle X-ray scattering (WAXS) analysis of ZnS nanoparticles. (a) The q-weighted structure factors for Samples 1−4, plotted with vertical offsets, ordered by increasing crystallinity. The diffraction vector, q, is defined in the text. (b) The corresponding real-space pair distribution functions (PDF). (c) Comparison of the experimental PDF of bulk cubic ZnS (dashed line), the simulated PDF of a 3.3−3.5 nm diameter nanoparticle with the bulk cubic ZnS structure (thick gray line), and the experimental PDF of 3.4 nm nanoparticles (thin black line, Sample 4). Data from Samples 2 and 3 were acquired in solution, resulting in poorer signal-to-noise than other samples measured as powders.

nanoparticles.[27] We observed previously that ZnS nanoparticles synthesized in water (sample 4) frequently contained stacking faults but mercaptoethanol coated nanoparticles (sample 1) contained many fewer stacking faults.[37] Phase analysis is challenging for sample 2 because of the extreme peak broadening. However, the XRD data are consistent with a highly strained sphalerite structure. The XRD data indicate no detectable bulk oxides in any sample.

The diffraction data additionally show that the samples possess a considerable range of internal structural disorder. Diffraction measurements on nanoparticles are sensitive to both particle size and disorder, both of which cause diffraction peak broadening. Because all of the samples contain nanoparticles of approximately the same size, the larger diffraction peak widths and lower PDF intensities can be attributed only to internal disorder. Provided the size is

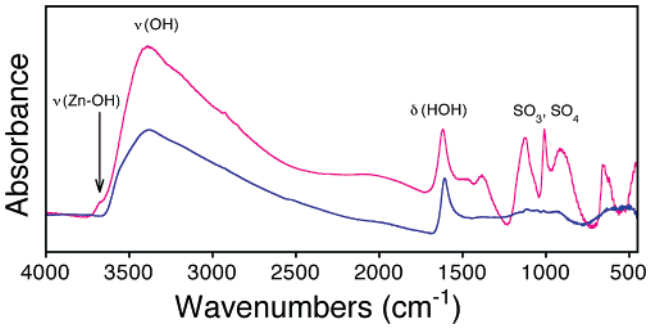

Figure 3. Fourier transform infrared spectra from ZnS nanoparticles synthesized in water at pH 11 (top, sample 4), and from nanoparticles synthesized in methanol, 24 h after the addition of water (bottom, sample 2).

determined independently (e.g., by SAXS), there is a straightforward method of separating the two contributions to the PDF data. The PDF displays all characteristic interatomic distances in a material: the shortest bond-length produces the first peak. In nanoparticles, the maximum interatomic distance that can contribute to the PDF is limited by the particle diameter. Although interatomic scattering may occur between atoms in different nanoparticles, the nanoparticles are on average not aligned with the precision of atoms in a crystal and so interparticle scattering does not contribute to the PDF and can be neglected. The effect of small particle size is therefore to contribute an envelope function in real space that reduces the PDF peak intensity at greater interatomic distance. For spherical nanoparticles, the finite size envelope function can be calculated analytically and provides a method to account quantitatively for finite size in PDF measurements.[18]

Figure 2c compares the PDF from sample 4 with a PDF simulated by applying an envelope function to the experimental PDF of bulk cubic ZnS. Because the simulation uses the experimental data for the bulk sample, rather than using a completely theoretical simulation, important experimental parameters, such as the energy resolution of the X-rays, are automatically included. To indicate how errors in nanoparticle size determination may affect this comparison, the simulated PDF is drawn as a broad line that encompasses the results for a range of diameters (3−3.8 nm). Figure 2c shows that when the finite particle size is considered, even the most crystalline of the samples studied contains more disorder than present in bulk ZnS, and most samples are considerably more disordered. There is evidently a relationship between surface ligand and interior structure, which we addressed further with FTIR spectroscopy.

Figure 3 compares the infrared spectra from samples 1 and 3; FTIR data for water binding are summarized for all samples in Table 2. All exhibit a broad absorption band in the 3000−3500 cm^{-1} region that is associated with ν(OH) stretching vibrations of liquid water with disordered hydrogen bonds. However, the δ(HOH) bending vibrations of molecular water appear at different positions, 1620 cm^{-1} for sample 4, and 1608 cm^{-1} for sample 3. In both cases, this vibration is shifted to lower wavenumbers with respect to pure liquid water (1638 cm^{-1}). The spectrum of sample 4 exhibits a

Table 2. Positions of Infrared Absorption Peaks Associated with Surface Hydroxyl Groups and Bound Molecular Water on ZnS Nanoparticles and Synthetic Bulk Cubic ZnS

	nanoparticles				bulk
sample number	1	2	3	4	5
surface coating	SHEtOH	methanol	water	oxidized	water
ν(Zn−OH)/cm^{-1}				3670	
δ(HOH)/cm^{-1}	1615		1608	1620	1638

relatively sharp ν(OH) stretching vibration at 3670 cm^{-1} that can be attributed to surface bound zinc hydroxyl groups,[41,42] that is not present in any other spectra. In addition, the group of peaks around 1000 cm^{-1} is indicative of sulfate groups.[41] Because there is no evidence of a distinct ZnO phase from any diffraction data, the FTIR data therefore indicate that the oxidized groups are confined to the nanoparticle surface. No other samples showed evidence of surface oxidation, indicating that it was not caused by the degassing procedure prior to FTIR analysis.

The shift of the δ(HOH) vibration to lower wavenumbers relative to liquid water is indicative of molecular water that is bound to a surface. This trend has been observed for water bound to nanoparticles of diamond[38] and for water in clays.[40] In our study, FTIR spectroscopy of synthetic bulk ZnS after the degassing procedure showed that this sample was not oxidized, and gave a δ(HOH) vibration at 1638 cm^{-1}. This value is identical to that for pure liquid water, as reported previously for water on bulk ZnS.[43] Hence, the binding of water to the surface of ZnS nanoparticles occurs at distinct sites from the surface of microscopic grains of cubic ZnS. The hexagonal and cubic phases of bulk ZnS possess different surface sites,[43] but neither the WAXS nor FTIR data can be explained by assuming that the nanoparticles have the hexagonal structure. Modified surface sites are commonly predicted for nanoparticles[44] and inferred from experimental studies.[19] Consequently, nanoparticles likely exhibit reconstructed, strained, or highly faceted surfaces. Alternatively, the electronic properties (e.g., Lewis acid strength) of binding sites may be modified in small particles because of boundary effects or more pervasive structural perturbations.

From the FTIR data, we can derive descriptions of the surfaces of each nanoparticle type. The observation of SH groups in the spectrum from sample 3 indicates that mercaptoethanol is bound electrostatically to surface zinc atoms, without deprotonation or formation of covalent thiol bonds to surface sulfur atoms. Molecular water is bound electrostatically to all samples, but dissociated water forms metal−hydroxyl groups at the surface of sample 4 only. The presence of sulfur oxides indicates partial oxidation of sample 4. Because this is not associated with sample handling after synthesis, and because separate oxide phases are not observed with X-ray diffraction, the partial oxidation is likely confined to the immediate surface.

We were not able to observe whether methanol has any significant surface bonding, but we anticipate weak surface interactions. Water binding stabilizes a more crystalline

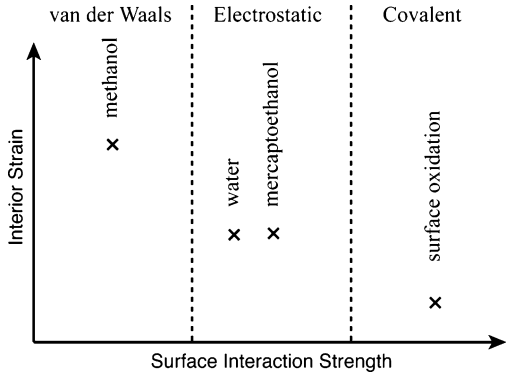

Figure 4. Scheme indicating the variation of strain within approximately 3 nm diameter ZnS nanoparticles for different surface interactions.

structure, similar to that stabilized by mercaptoethanol. Both of these species are believed to bind electrostatically to surface zinc atoms, leaving sulfur atoms underbonded. The structure with water is slightly more crystalline than that with mercaptoethanol, suggesting that stearic hindrance of the larger mercaptoethanol molecules allows binding to fewer surface atoms. Both covalent binding of hydroxyl to zinc and the presence of oxidized sulfur atoms result in the most crystalline material of all. For II−VI semiconductor nanoparticles, electrostatic passivation of surface cations by negatively charged ligands has generally been employed.[13,46] Passivation of surface anions is much less well studied (see ref 47). Our results indicate that capping nanoparticle surfaces so that both surface anion and cations are fully bonded will produce the most crystalline nanoparticles. The core−shell structures obtained by growing a second semiconductor material after nanoparticle synthesis, such as ZnS shells on CdSe nanoparticles, are examples of the most complete surface bonding that can be attained. In such cases, however, lattice mismatch can cause strain within the core.[48]

Conclusions. We combined PDF analysis of nanoparticle structure with particle size analysis to provide a measure of the crystallinity of nanoparticles (although obtaining real-space representation of nanoparticle structure remains a challenge). We show that the crystallinity of ZnS nanoparticles can fall within a large continuum and that the nature of the surface chemical interactions appears to be the dominant factor in determining the extent of interior disorder. In our study, the most crystalline nanoparticles are those with strong covalent termination.

Our method may be used to determine the extent to which disorder is present within nanoparticles that exhibit high-quality optical properties, such as band edge emission and high fluorescent yields, and the consequences of the disorder on these properties. No effort was made here to optimize or measure the optical properties of the nanoparticle samples. Nevertheless, Figure 4 indicates that the effectiveness of nanoparticle capping agents may be more linked to the removal of surface trap states than the imposition of bulklike crystallinity.

Although the present study addresses the effect of surface chemistry only, we expect that the disorder will exhibit a strong dependence on particle size because preliminary data show that approximately 6 nm diameter ZnS particles are far less disordered than the 3−4 nm nanoparticles reported here.[49]

Acknowledgment. Small-angle X-ray scattering data were acquired at beamline 5-ID-D of the Advanced Photon Source (APS) with the support of Steve Weigand, and at beamline 1-4 at the Stanford Synchrotron Radiation Laboratory with the support of John Pople. Wide-angle X-ray scattering data were acquired at beamline 11-ID-B at the APS with the support of Yang Ren. TEM data were acquired at the National Center for Electron Microscopy with the support of Chegyu Song. We thank Michael Martin for access to the Nicolet FTIR spectrometer. Funding for this work was provided by a grant from the Department of Energy Chemical Sciences Program ER 15218 and the National Science Foundation NIRT program EAR0123967 and by the Director, Office of Science, of the U.S. Department of Energy under Contract no. DE-AC02-05CH11231.

Supporting Information Available: High-resolution transmission electron microscope images of each of the nanoparticle samples that verify the particle size determined with small-angle X-ray scattering. This material is available free of charge via the Internet at http://pubs.acs.org.

References

(1) Alivisatos, A. P. *Science* **1996**, *271*, 933.
(2) Murray, C. B.; Norris, D. J.; Bawendi, M. G. *J. Am. Chem Soc*. **1993**, *115*, 8706.
(3) Ranade, M. R.; Navrotsky, A.; Zhang, H. Z.; Banfield, J. F.; Elder, S. H.; Zaban, A.; Borse, P. H.; Kulkarni, S. K.; Doran, G. S.; Whitfield, H. J. *Proc. Natl. Acad. Sci. U.S.A.* **2002**, *99* (Suppl. 2), 6476.
(4) Zhang, H.; Banfield, J. F. *J. Mater. Chem.* **1998**, *8*, 2073.
(5) Leung, K.; Whaley, K. B. *J. Chem. Phys.* **1999**, *110*, 11012.
(6) Wang, L.-W.; Zunger, A. *Phys. Rev. B* **1996**, *53*, 9579.
(7) Rabani, E. *J. Chem. Phys*. **2001**, *115*, 1493.
(8) Puzder, A.; Williamson, A. J.; Reboredo, F. A.; Galli, G. *Phys. Rev. Lett*. **2003**, *91*, 157405.
(9) Zhang, H.; Gilbert, B.; Huang, F.; Banfield, J. F. *Nature* **2003**, *424*, 1025.
(10) Gilbert, B.; Huang, F.; Zhang, H.; Ren, Y.; Haskel, D.; Lang, J. C.; Srajer, G.; Jürgenssen, A.; Waychunas, G. A.; Banfield, J. F. *J. Chem. Phys*. **2004**, *120*, 11785.
(11) Kumpf, C.; Neder, R. B.; Niederdraenk, F.; Luczak, P.; Stahl, A.; Scheuermann, M.; Joshi, S.; Kulkarni, S. K.; Barglik-Chory, C.; Heske, C.; Umbach, E. *J. Chem. Phys.* **2005**, *123*, 224707.
(12) Stoneham, A. M. *Theory of Defects in Solids;* Clarendon Press: Oxford, 1985.
(13) Hellmann, R.; Euteneuer, A.; Hense, S. G.; Feldmann, J.; Thomas, P.; Göbel, E. O.; Yakovlev, D. R.; Waag, A.; Landwehr, G. *Phys. Rev. B* **1995**, *51*, 18053.
(14) Rockenberger, J.; Tröger, L.; Rogach, A. L.; Tischer, M.; Grundmann, M.; Eychmüller, A.; Weller, H. *J. Chem. Phys.* **1998**, *108*, 7807.
(15) Marcus, M. A.; Flood, W.; Steigerwald, M.; Brus, L.; Bawendi, M. G. *J. Phys. Chem*. **1991**, *95*, 1572.
(16) Carter, A. C.; Bouldin, C. E.; Kemner, K. M.; Bell, M. I.; Woicik, J. C.; Majetich, S. A. *Phys. Rev. B* **1997**, *55*, 13822.
(17) Bawendi, M. G.; Kortan, A. R.; Steigerwald, M. L.; Brus, L. E. *J. Chem. Phys.* **1989**, *91*, 7282.
(18) Vogel, W.; Urban, J.; Kundu, M.; Kulkarni, S. K. *Langmuir* **1997**, *13*, 827.
(19) Gilbert, B.; Huang, F.; Zhang, H.; Waychunas, G. A.; Banfield, J. F. *Science* **2004**, *305*, 651.
(20) Son, D. H.; Hughes, S. M.; Yin, Y.; Alivisatos, A. P. *Science* **2004**, *306*, 1009.

(21) Huang, F.; Gilbert, B.; Zhang, H.; Banfield, J. F. *Phys. Rev. Lett.* **2004**, *92*, 155501.
(22) Banfield, J. F.; Welch, S. A.; Zhang, H.; Ebert, T. T.; Penn, R. L. *Science* **2000**, *289*, 751.
(23) Penn, R. L.; Banfield, J. F. *Am. Mineral.* **1999**, *84*, 871.
(24) Tang, Z.; Kotov, N. A.; Giersig, M. *Science* **2002**, *297*, 237.
(25) Rajh, T.; Chen, L. X.; Lukas, K.; Liu, T.; Thurnauer, M. C.; Tiede, D. M.; *J. Phys. Chem. B* **2002**, *106*, 10543.
(26) Wuister, S. F.; Donega, C. M.; Meijerink, A. *J. Am. Chem. Soc.* **2004**, *126*, 10397.
(27) Vogel, W.; Borse, P. H.; Deshmukh, N.; Kulkarni, S. K. *Langmuir* **2000**, *16*, 2032.
(28) Hammerly, A. P. Fit2D. *Internal Report ESRF98HA01T*; European Synchrotron Radiation Facility: Grenoble, France.
(29) Hamad, S.; Cristol, S.; Catlow, C. R. A. *J. Phys. Chem.* **2002**, *106*, 11002.
(30) Kotlarchyk, M.; Chen, S.-H. *J. Chem. Phys.* **1983**, *79*, 2461.
(31) Gazzillo, D.; Giacometti, A. *J. Chem. Phys*. **2000**, *113*, 9837.
(32) Teixeira, J. *J. Appl. Crystallogr*. **1988**, *21*, 781.
(33) Chupas, P. J.; Qiu, X.; Hanson, J. C.; Lee, P. L.; Grey, C. P.; Billinge, S. J. L. *J. Appl. Crystallogr.* **2003**, *36*, 1342.
(34) Thijsse, B. J. *J. Appl. Crystallogr*. **1984**, *17*, 61.
(35) Egami, T. *Local Structure from Diffraction*; Billinge, S. J. L., Thorpe, M. F., Eds.; Plenum, New York, 1998; p 1.
(36) Toby, B. H.; Egami, T. *Acta Crystallogr*. **1992**, *A48*, 336.
(37) Huang, F.; Zhang, H.; Banfield, J. F. *J. Phys. Chem. B* **2003**, *107*, 10470.
(38) Guinier, A. *X-ray Diffraction in Crystals, Imperfect Crystals and Amorphous Bodies*; W. H. Freeman & Co.: San Francisco, CA, 1963.
(39) Ji, S.; Jiang, T.; Xu, K.; Li, S. *Appl. Surf. Sci.* **1998**, *133*, 231.
(40) Johnston, C. T.; Sposito, G.; Erickson, C. *Clays Clay Miner*. **1992**, *40*, 722.
(41) Little, L. H. *Infrared Spectra of Adsorbed Surface Species*; Academic Press: New York, 1966.
(42) Koretsky, C. M.; Sverjensky, D. A.; Salisbury, J. W.; D'Aria, D. M.; *Geochim. Cosmochim. Acta* **1997**, *61*, 2193.
(43) Hertl, W. *Langmuir* **1988**, *4*, 594.
(44) Puzder, A.; Williamson, A. J.; Gygi, F.; Galli, G. *Phys. Rev. Lett.* **2004**, *92*, 217401.
(45) FTIR analysis of ZnS nanoparticles in pure methanol gave quantitatively similar results to nanoparticles in methanol following the addition of water. Trace water in solution was evidently concentrated during drying.
(46) Vossmeyer, T.; Katsikas, L.; Gienig, M.; Popovic, I. G.; Diesner, K.; Chemseddine, A.; Eychmiiller, A.; Weller, H. *J. Phys. Chem.* **1994**, *98*, 7663−7673.
(47) Ni, T.; Nagesha, D. K.; Robles, J.; Materer, N. F.; Müssig, S.; Kotov, N. A. *J. Am. Chem. Soc.* **2002**, *124*, 3980−3992.
(48) Little, R. B.; El-Sayed, M. A.; Bryant, G. W.; Burke, S. *J. Chem. Phys.* **2001**, *114*, 1813−1822.
(49) Gilbert, B., unpublished data.

NL052201C